

Structural evolution in synthetic, Ca-based sorbents for carbon capture



Wen Liu^{a,*}, Belén González^b, Matthew T. Dunstan^c, D. Saquib Sultan^b, Adriano Pavan^d,
Chris D. Ling^d, Clare P. Grey^c, J.S. Dennis^b

^a Cambridge Centre for Advanced Research in Energy Efficiency in Singapore, Nanyang Technological University, Singapore 637459, Singapore

^b University of Cambridge, Department of Chemical Engineering and Biotechnology, Cambridge CB2 3RA, United Kingdom

^c University of Cambridge, Department of Chemistry, Cambridge CB2 1EW, United Kingdom

^d School of Chemistry, University of Sydney, Sydney, New South Wales 2006, Australia

HIGHLIGHTS

- The Ca-based synthetic sorbents shows improving performance with cycling.
- The performance of the synthetic sorbents depends on their cycling history.
- The effect of cycling history on the sorbent's performance is cumulative.
- A surface cracking model explains the behaviour of the sorbent over cycling.
- The reaction model proposed maybe applicable to natural sorbents.

ARTICLE INFO

Article history:

Received 26 June 2015

Received in revised form

15 September 2015

Accepted 17 September 2015

Available online 26 September 2015

Keywords:

Carbon dioxide

Absorption

Reaction engineering

Materials

Sintering

ABSTRACT

The carbonation of CaO-based materials at high temperatures (*e.g.* > 600 °C) is a promising method of capturing CO₂ emitted from, *e.g.* the combustion of carbonaceous fuels. The resulting CaCO₃ can be regenerated by calcination at a temperature at which the equilibrium partial pressure exceeds that of the local partial pressure of CO₂ (*e.g.* 950 °C). A process involving repeated cycles of carbonation and calcination of a calcareous material is called calcium looping. The capacity of a CaO-based sorbent to accept and reject CO₂ over many cycles is governed by a number of factors, such as chemical composition, surface morphology and pore structure, all of which often evolve with cycling. The present paper investigates the underlying mechanisms controlling the evolution of the micro-structures of a series of synthetic sorbents consisting of CaO mixed with the inert supports Ca₁₂Al₁₄O₃₃ and MgO. These sorbents were subjected to cycles of calcination and carbonation and were characterised using a variety of *in situ* and *ex situ* techniques. It was found that the balance between the degree of surface cracking during calcination and the extent of sintering during carbonation was responsible for changes in uptake during cycling, giving an increase in uptake for the supported CaO and a decrease for the unsupported CaO.

© 2015 The Authors. Published by Elsevier Ltd. This is an open access article under the CC BY license (<http://creativecommons.org/licenses/by/4.0/>).

1. Introduction

This paper is concerned with the capture of CO₂ from combustion flue gases using solid sorbents containing CaO, and the calcination of the resulting CaCO₃ to regenerate the sorbent and to produce a stream of pure CO₂ suitable for sequestration in the Earth. A major advantage of using calcium-based sorbents is the high temperature at which the system operates, meaning that heat rejected during the exothermic carbonation can produce useful work. This makes calcium-based carbon capture

substantially more efficient than low-temperature technologies, *e.g.* adsorption using molecular sieves or absorption in an amine solvent, all of which reject heat at low temperature, with a consequent low potential for undertaking work, during the uptake of CO₂.

During continuous operation, a calcium-based sorbent would be subjected to cycles consisting of carbonation by CO₂ to CaCO₃ followed by calcination of the CaCO₃ to CaO, a process called “calcium looping”. The rate of carbonation is highly dependent on the surface area and the pore structure of the solid reactant. It has been widely reported that the carbonation of CaO occurs in two stages: an initial fast stage followed by a slow stage, which is believed to be controlled by the diffusion of CO₂ through the

* Corresponding author.

E-mail address: w1247@cam.ac.uk (W. Liu).

product layer of CaCO_3 (Abanades and Alvarez, 2003; Barker, 1973; Bhatia and Perlmutter, 1983; Gupta and Fan, 2002).

Generally, the theoretical stoichiometric uptake of 0.79 g CO_2/g CaO is almost never achieved. Also, natural sorbents, e.g. limestones, lose reactivity rapidly after only a few cycles of carbonation and calcination, because both the surface area and porosity of the material decrease irreversibly as a result of sintering (Anthony, 2008; Fennell et al., 2007). For example, after 20 cycles of carbonation and calcination, the capacity of limestone for CO_2 drops to ~20% of its initial value (Fennell et al., 2007). To overcome the problem of deactivation, synthetic calcium-based sorbents have been investigated, aiming at maintaining a high capture capacity over many cycles of carbonation and calcination.

Li et al. (2005) investigated synthetic sorbents made by mixing powdered CaO with a ceramic binder, mayenite, ($\text{Ca}_{12}\text{Al}_{14}\text{O}_{33}$) in mass ratios of up to 3:1, by a hydrolysis method, and compared their performance to pure CaO and three natural sorbents, all of which contained > 98 wt% CaCO_3 . During 13 cycles of carbonation and calcination in a thermogravimetric analyser (TGA), it was found that the synthetic $\text{CaO-Ca}_{12}\text{Al}_{14}\text{O}_{33}$ sorbent and the dolomites exhibited lower rates of deactivation than pure CaO. Li et al. (2005) concluded that the mayenite increased the stability of the reactivity by preventing sintering, agreeing with the findings of Silaban et al. (1996).

Pacciani et al. (2008a) synthesised sorbents based on mixtures of CaO with either mayenite or MgO, prepared by either (i) the hydration of CaO in a solution of Al or Mg nitrate or (ii) the coprecipitation of soluble salts of each component, followed in both cases by calcination at high temperature. The ability of such sorbents to absorb CO_2 , compared with limestone and dolomite, over cycles of carbonation and calcination was examined in a laboratory-scale fluidised bed. After 20 cycles, it was found that CaO in admixture with mayenite, synthesised by hydration of CaO, exhibited the least attrition amongst the synthetic sorbents. This toughening effect was thought to be due to the hardness of the mayenite. Furthermore, after 20 cycles, two of the synthetic sorbents, containing 75 wt% and 85 wt% CaO, respectively, showed a higher uptake of CO_2 per mole of CaO than the limestone, for a fixed carbonation time.

Broda et al. (2012) and Broda and Müller (2012) synthesised CaO-based sorbents supported on $\text{Ca}_{12}\text{Al}_{14}\text{O}_{33}$ via either a sol-gel route or a carbon gel route. Their sorbents showed stable performance over cycling in a TGA. Furthermore, they observed that the rate of carbonation of the supported sorbents also exhibits a two-stage behaviour.

Dennis and Pacciani (2009) studied the effect of variations in the partial pressure of CO_2 , p_{CO_2} , on the extent of uptake of CO_2 by a natural sorbent (Steetley dolomite) and a synthetic one (85 wt% CaO and 15 wt% mayenite, named HA-85-850). They found that an increase in p_{CO_2} , from 0.15 to 0.8 bar during carbonation, did not have a significant impact on the uptake by the dolomite, whereas the ultimate uptake by the synthetic sorbent increased markedly. To explain this difference, Dennis and Pacciani (2009) proposed that the uptake during the slow stage is determined thermodynamically by the p_{CO_2} of the reacting gas. However, Liu et al.

(2012b) later suggested that the slow stage is controlled by product layer diffusion, so that the increase in the uptake with p_{CO_2} is, in fact, a kinetic effect and dependent on the pore structure of the sorbent.

The objective of the present work is to investigate the mechanisms determining the variation in uptake of CO_2 by synthetic sorbents of CaO supported on $\text{Ca}_{12}\text{Al}_{14}\text{O}_{33}$ and MgO on cycling. In particular, how the operating conditions during carbonation influence the behaviour of the sorbents in the subsequent cycles is examined experimentally.

2. Experimental

2.1. Material synthesis

The calcium-based sorbents consisted of oxides of calcium, magnesium, aluminium and mixed oxides formed therefrom. The starting reagents were powdered CaO (97+wt% purity, for analysis, Acros Organics), $\text{Mg}(\text{NO}_3)_2 \cdot 6\text{H}_2\text{O}$ (99.0+wt% purity, Fluka Analytical), $\text{Al}(\text{NO}_3)_3 \cdot 9\text{H}_2\text{O}$ (laboratory reagent grade, Fisher Scientific) and propan-2-ol (laboratory reagent grade, Fisher Scientific).

Samples were prepared using the hydrolysis method adapted from Li et al. (2005). In a typical synthesis, powdered CaO, Al ($\text{NO}_3)_3 \cdot 9\text{H}_2\text{O}$ and $\text{Mg}(\text{NO}_3)_2 \cdot 6\text{H}_2\text{O}$ were added in turn to a mixture of 75 vol% water, 25 vol% propan-2-ol agitated vigorously at 75 °C. The molar ratio of Mg:Al was fixed at 1:2 in all samples whilst the amount of the active component, CaO, was varied. Stirring was continued at the same temperature for 1 h. The resulting slurry was dried overnight at 120 °C in an atmospheric oven where all the water was evaporated. The dried cake was calcined in air at 850 °C for 3 h, crushed and sieved to desired size fractions. According to calculations using the thermodynamic software package MTDATA, using the NPL Oxide database (Davies et al., 2002), the synthetic sorbents should consist of three components, viz. CaO, $\text{Ca}_{12}\text{Al}_{14}\text{O}_{33}$ and MgO, which are thermodynamically stable and mutually insoluble at 850 °C in air. Therefore, the sorbents were named with the prefix “HAM”, to denote the method of hydrolysis of CaO with the addition of aluminium and magnesium, followed by a number indicating the mass percentage of CaO; the exact compositions of the four synthetic sorbents are tabulated in Table 1.

2.2. Thermogravimetric analysis (TGA)

When the rate of reaction is slow, the kinetics are best studied in a thermogravimetric analyser (here, a TGA/DSC 1, Mettler-Toledo was used). In a typical experiment, 5.0–10.0 mg of sample was placed in an alumina crucible, which was continuously weighed by a cantilever micro-balance. The mass of sample was selected such that it gave an approximate monolayer of particles covering the base of the crucible. The gas flow arrangement for the TGA is identical to that depicted in Fig. 2 of Liu et al. (2012b). The reactive gas, prepared by mixing pure CO_2 and N_2 from

Table 1
Composition of the synthetic sorbents, expressed in mass fraction, mole fraction and mole fraction of Ca.

Sorbents composition	CaO			$\text{Ca}_{12}\text{Al}_{14}\text{O}_{33}$			MgO		
	wt%	mol%	Ca mol%	wt%	mol%	Ca mol%	wt%	mol%	Ca mol%
HAM100	100	100	100	0	0	0	0	0	0
HAM83	83	94.9	92.5	14	0.6	7.5	3	4.5	0
HAM66	66	88.1	83.1	28	1.5	16.9	6	10.4	0
HAM50	50	78.6	71	42	2.7	29	8	18.7	0

compressed gas cylinders, was fed into the reacting chamber of the TGA at a total rate of 50 ml min^{-1} (STP). To ensure the quality of the gas mixture, CO_2 and N_2 were firstly mixed to give a total flowrate of 200 ml min^{-1} (STP), of which 50 ml min^{-1} was passed into the TGA and the remainder passed through a NDIR gas analyser (EL3020 Uras 26, ABB) to measure the partial pressure of CO_2 in the reactive gas. Based on a preliminary measurement, it takes 25 s for the concentration in the outlet to reach 90% of the inlet following a step change in the inlet.

During a typical experiment, the sorbent was cycled between a carbonating and a calcining environment by switching the inlet gas whilst keeping the temperature constant at 750°C . During carbonation the reactive gas mixture was fed at 50 ml min^{-1} (STP). During calcination the reactive gas was switched off, and the sample was exposed to a constant purge of N_2 at a flow rate of 20 ml min^{-1} . To investigate the behaviour of the sorbent over multiple cycles, each sorbent was carbonated for 40 min and then calcined for 20 min, 100 times. The relatively long carbonation time was chosen in order to investigate (i) the rate of the slow stage and (ii) the effect of prolonged carbonation.

2.3. Fluidised bed experiments

The synthetic sorbents were also investigated in a laboratory-scale fluidised bed reactor, by undertaking repeated cycles of carbonation (for 480 s) and calcination (for 480 s). These reaction times were used by Pacciani et al. (2008a) when investigating synthetic sorbents and were found to be ample for complete carbonation in the fast stage and subsequent full calcination at 750°C . The arrangement of the apparatus was identical to that used by Pacciani et al. (2008a). In each experiment, a batch of $\sim 1 \text{ g}$ (calcined basis) of fresh sorbent, $1.7 < d_p < 2.3 \text{ mm}$, was mixed with 20 ml (untapped volume) of silica sand, $500 < d_p < 710 \mu\text{m}$, in a quartz reactor of $I.D.=30 \text{ mm}$. The bed was heated by an external electric furnace to 750°C and fluidised by mixtures of nitrogen and CO_2 , made by mixing gases from cylinders of pure N_2 and pure CO_2 (Air Liquide). During calcination, the bed was fluidised by N_2 at a flowrate of 60 ml s^{-1} (STP). During carbonation, the bed was fluidised by 10.6, 25.8 or 60 ml s^{-1} (STP) of CO_2 in addition to 60 ml s^{-1} (STP) N_2 , resulting in a mole fraction of CO_2 of 15, 30 or 50% CO_2 , respectively, in the reactive reacting gas. Such flowrates corresponded to $U/U_{mf}=2.3$ during calcination and $U/U_{mf}=2.7, 3.2$ and 4.5 during carbonation in 15%, 30% and 50% CO_2 , respectively. Here, the value of U_{mf} was calculated from the correlation of Wen and Yu (1966). By measuring continuously the off-gas composition of the fluidised bed using a non-dispersive infrared analyser (EL 2030, URAS26, ABB), the rate and extent of uptake of CO_2 by the sorbent was calculated using the analysis of Pacciani et al. (2008a).

2.4. In situ synchrotron X-ray diffraction

The change in composition of the crystalline phase of the synthetic sorbent was investigated by measuring *in situ* the X-ray diffraction patterns of HAM83 during one cycle of carbonation and calcination on the PD beamline of the Australian Synchrotron. Variable-temperature synchrotron XRD (sXRD) measurements were collected using a wavelength $\lambda=0.82354 \text{ \AA}$. Samples were placed in quartz capillaries, 0.5 mm diameter, and mounted in a gas-flow cell. First, measurements were taken at room temperature. Then, the sample was heated to 900°C at a rate of 5°C min^{-1} under flowing CO_2 . The sample was held at 900°C , and measurements were made continuously and isothermally for 1 h (10 scans, each taking 6 min); then the gas flow was switched to N_2 and measurements were again made continuously for 1 h. The flowrates of N_2 and CO_2 were both about 25 ml min^{-1} (STP).

Finally, the sample was cooled to 600°C and the gas flow was switched back to CO_2 and measurements again made for another hour. The time taken for cooling down was about 10 min, during which time scanning was halted until reaching the new set-point temperature of 600°C . The collected diffractograms were analysed by Rietveld refinement using GSAS (Larson and Von Dreele, 2000) with the graphical interface EXPGUI (Toby, 2001). The phase composition of the sample was estimated using the results of the refinement.

2.5. Ex situ characterisation

The exteriors of the sorbents, before and after the cycling experiments, were examined using a scanning electron microscope (Field Emission SEM, JOEL-6340F). Electron micrographs were collected using secondary electron imaging (SEI) with an accelerating voltage of up to 15 kV. The specific surface area and pore volumes of the samples were determined based on the BET and BJH models (Barrett et al., 1951; Brunauer et al., 1938), using the nitrogen adsorption–desorption isotherms measured by a BET analyser (Tristar 3000, Micrometrics Instrument) at 77 K.

3. Results

3.1. In situ synchrotron X-ray diffraction of HAM83

The evolution of the composition of the crystalline phases in HAM83 over one cycle, measured by *in situ* sXRD, is shown in Fig. 1. Fig. 1 shows that full carbonation was achieved during the heating of HAM83 to 900°C in CO_2 , so at $t=108 \text{ min}$ the HAM83 consisted of calcite (CaCO_3) and mayenite ($\text{Ca}_{12}\text{Al}_{14}\text{O}_{33}$). After switching the inlet gas to N_2 , the CaCO_3 quickly decomposed, giving rise to peaks of CaO . After $t=222 \text{ min}$, the sample was cooled to 600°C and reacted with pure CO_2 , converting most of the CaO back to CaCO_3 . In all diffraction patterns, only weak peaks of mayenite ($\text{Ca}_{12}\text{Al}_{14}\text{O}_{33}$) were detected, owing to the relatively low abundance of this phase. It should also be noted that the

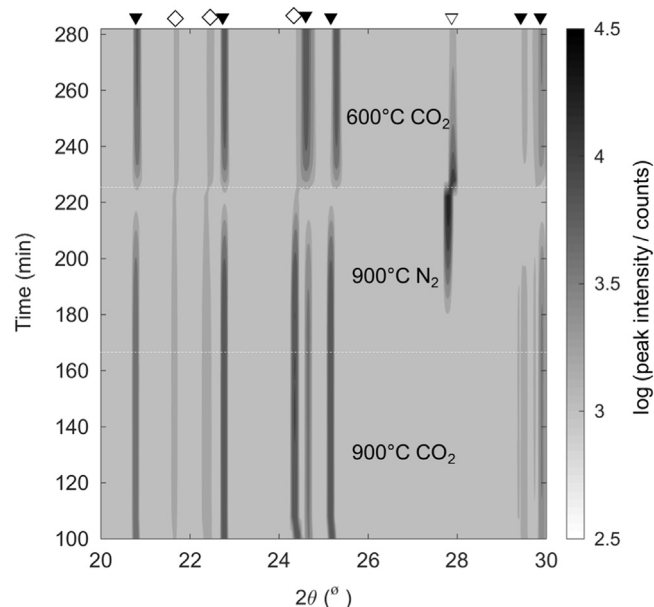


Fig. 1. Contour plot of *in situ* sXRD patterns of HAM83 over one cycle of calcination–carbonation. The intensities (in logarithmic scale) correspond to peak intensities on the diffraction patterns. Only peaks between 20° and 30° are shown for brevity. All peaks are labelled with ∇ - CaCO_3 , \triangle - CaO and \diamond - $\text{Ca}_{12}\text{Al}_{17}\text{O}_{33}$. The first scan at 900°C was taken at $t=108 \text{ min}$.

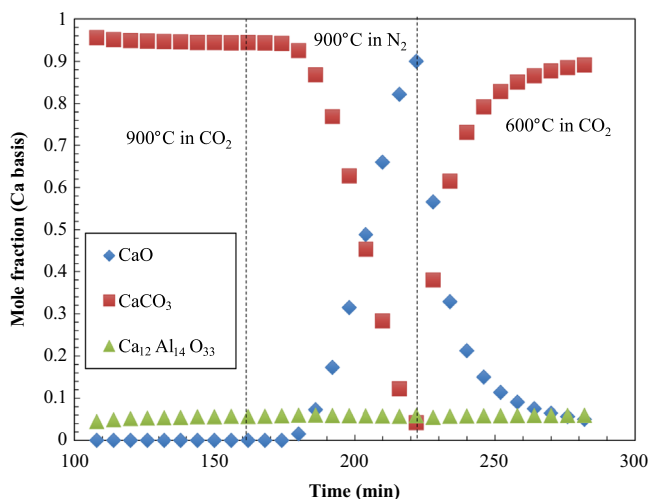


Fig. 2. Results of quantitative phase analysis of the *in situ* sXRD results for HAM83 over one cycle of carbonation–calcination. The first points at 108 min corresponds to the first collection of pattern at 900 °C. The interval between each XRD measurement is 6 min. Error bars determined from the Rietveld refinements are too small to be shown.

positions of all the peaks shift to higher 2θ from 900 °C to 600 °C owing to the effects of thermal contraction.

A quantitative analysis of the crystalline phase composition was performed using Rietveld refinement. Results are shown in Fig. 2, which indicates that all the CaO in the freshly-calcined HAM83 is convertible to CaCO₃. Overall, the estimated compositions of the synthetic sorbents are in agreement with those calculated in Section 2.1. The approximately constant mole fraction of mayenite suggests that it remained unreactive over the cycle in which almost full conversion from CaCO₃ to CaO and back to CaCO₃ was achieved. On average, the mole fraction of mayenite is $\sim 5.6 \pm 0.3\%$ (Ca basis), lower than the expected value of 7.5% in Table 1. This discrepancy is comparable with typical uncertainties expected for quantitative phase analysis by Rietveld refinement, e. g. 2 mol%. However, MgO was not detected in any experiment. Here, the possibility of MgO dissolving in CaO is ruled out because it is thermodynamically infeasible below 1600 °C (Doman et al., 1963). Therefore, the failure to detect MgO is probably because either it is poorly crystalline or composed of particles too small to give good coherent diffraction.

3.2. Fluidised bed experiments

For the cycling experiments in the fluidised bed, the uptakes were estimated based on the amounts of CO₂ released during the calcinations. Then, the uptake was normalised to conversion, X , the mole fraction of CaO converted to CaCO₃ at the end of the carbonation. Fig. 3 shows the analysed results of the cycling experiments; it can be seen that, amongst the freshly-calcined samples, HAM100 shows the highest conversion of 0.43. However, this value dropped steadily over cycles, reaching 0.22 at the 100th cycle. The behaviour of HAM100 is similar to that commonly observed for natural Ca-based sorbents, which usually contain > 90 wt% CaO and CaCO₃ and decay in performance quickly. In contrast, the three sorbents supported on MgO and mayenite started with low uptakes, which were almost doubled by the 100th cycle. Analogous behaviour has been reported by Pacciani et al. (2008a) and Stendardo et al. (2013), using sorbents of similar compositions. Overall, the most reactive sorbent was HAM83, with a conversion of 25% in the 100th cycle.

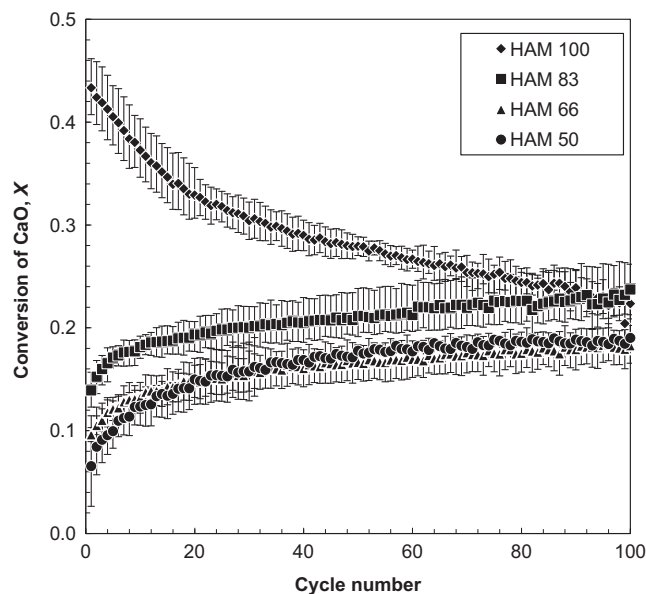


Fig. 3. Conversion of CaO versus cycle number, for four different synthetic sorbents cycled isothermally in a fluidised bed at 750 °C. In each cycle, the fluidised bed was first exposed to N₂ for 8 min and then 15% CO₂ (balance N₂) for 8 min. Error bars shown represent the maximum and minimum values from the set of three repeated experiments for each sorbent.

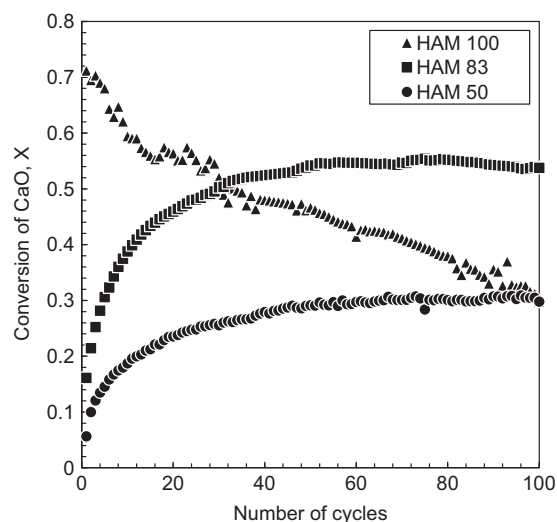


Fig. 4. Conversion of CaO versus number of carbonation–calcination cycles for different CaO-based synthetic sorbents. The sorbents were cycled isothermally at 750 °C. In each cycle the material was calcined in N₂ for 20 min and carbonated in 15% CO₂ in N₂ for 40 min.

3.3. TGA experiments

The TGA was particularly useful for studying the slow stage during carbonation, the rate of which is too slow to be measured by the gas analysers in a fluidised bed experiment described in Section 2.3. In addition, the TGA allows experimental investigation in the absence of artefacts such as attrition and elutriation.

Fig. 4 shows the results of cycling HAM50, 83 and 100 in the TGA when the carbonating gas was 15% CO₂ in N₂. The trends seen in Fig. 4 are similar to those in Fig. 3, but with higher uptakes, owing to the longer carbonation time. For HAM 100, X drops from 0.71 in the first cycle to 0.31 after 100 cycles, whereas for HAM83 and 50 the value of X increases drastically with cycling. Both curves for HAM83 and 50 appear to be reaching a plateau

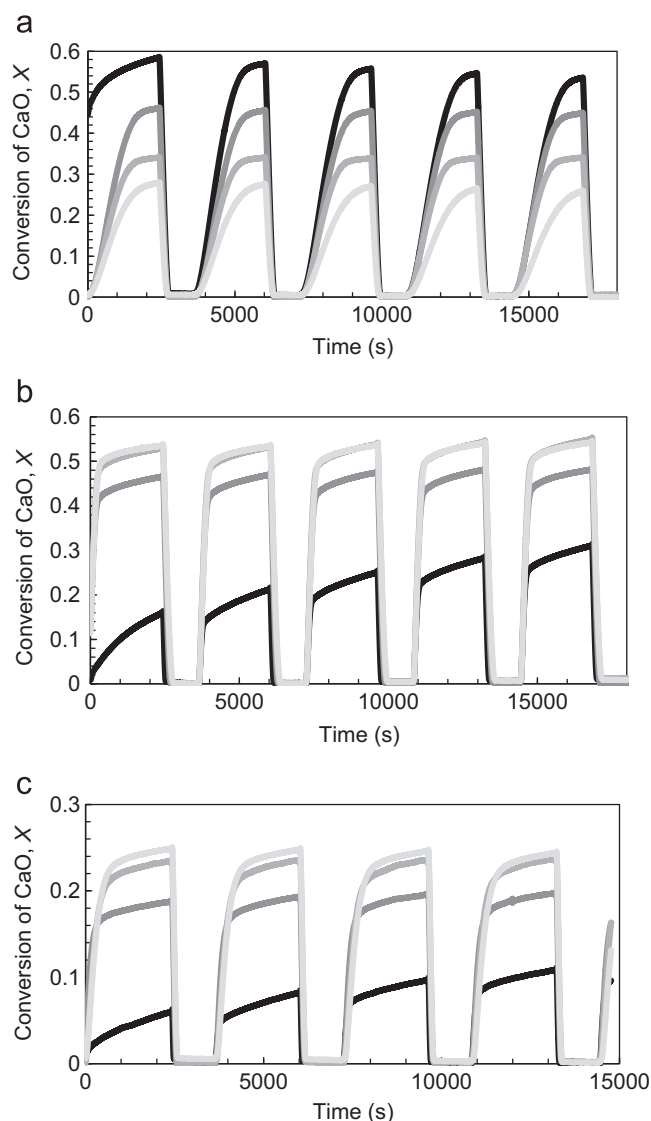


Fig. 5. Conversion of CaO as a function of time in a TGA for HAM100 (a), HAM83 (b) and HAM50 (c), during cycle numbers 1–5, 21–25, 61–65 and 96–100 in a TGA at 750 °C. During carbonation and calcination the reactive gas was 15% CO₂ in N₂ and N₂, respectively. Curves with lighter grey scales correspond to higher cycle numbers. For example, the curves in black correspond to results for cycle number 1–50 and the curves in the lightest grey correspond to results for cycle number 96–100.

towards the end of the experiment. Here, the uptake by HAM83 overtook that by HAM100 after 30 cycles, whereas in the fluidised bed, this occurred after 90 cycles. Again, this difference is a result of the long carbonation time used in the TGA.

The changes in X as a function of time during the TGA cycling experiments are shown in Fig. 5. For HAM100, there is little distinction between a fast and a slow stage during carbonation in the first five cycles, as shown in Fig. 5(a). With cycling, the apparent rate of carbonation continues to decay. In fact, at any given conversion, the rate slows with cycles. For cycles 21–25 and 61–65, there appears to be a transition from a fast stage to a slow stage during carbonation. However, this feature was not obvious for cycles 1–5 or 96–100.

Fig. 5(b) and (c) shows the results for HAM83 and 50, respectively. For both synthetic sorbents, an initial fast stage of reaction followed by a distinctly slower stage of reaction can be seen. For all cycles, the gradients of the conversion profiles of different cycles look similar at any given time except for the

point at which the fast stage changes to the slow stage. Also, the fast stage only lasts for a short period of time compared to the slow stage and is responsible for the majority of the uptake during carbonation. Over cycling, the fast stage persists for longer, resulting in an increase in the overall conversion, which stabilises after about 65 cycles. Similar behaviour is displayed by HAM50, showing a growing fast stage, and a slow stage with rates independent of the fast stage. The main differences between HAM50 and 83 are the lower overall conversions for HAM50 and the continuous growth of cyclic uptake throughout the 100 cycles, as shown in Fig. 5(c).

Fig. 5 also shows little change in the sorbents' behaviour during calcination, which goes to completion rapidly, agreeing with Barker (1973). Therefore the factor limiting the final CO₂ uptake in each cycle is the kinetics during carbonation, particularly the duration of the fast stage.

3.4. Effect of partial pressure of CO₂

The results suggest that HAM 83 was the best-performing sorbent over 100 cycles. This finding is in agreement with Paciani et al. (2008a), who reported that 85 wt% CaO supported on mayenite performed the best in their experimental series, despite the low uptake in the first cycle. Therefore, HAM 83 was chosen for further investigation.

After 60 cycles in a fluidised bed under conditions described in Section 2.3, a batch of HAM83 was recovered and cycled further in a TGA. Firstly, the recovered sorbents were carbonated in 70 mol% CO₂ in N₂ for 40 min followed by calcination in N₂ for 20 min for 10 cycles. Then, the material was cycled 10 more times with identical carbonation and calcination times, but changing the carbonating gas to 15 mol% CO₂ in N₂. The results are shown in Fig. 6. From Fig. 6(a) it can be seen that, with 70 mol% CO₂, X rose from 0.33 to 0.55 during the first 10 cycles. When the concentration of CO₂ was reduced to 15%, X dropped gradually over cycles, from 0.53 in the 11th cycle to 0.48 in the 20th. This suggests that the cyclic uptake of HAM83 is correlated with the carbonating p_{CO_2} in the current cycle, as well as the preceding ones. From Fig. 6(b), it can be seen that the sample recovered from the fluidised bed cycling experiment also carbonates in two stages. With identical p_{CO_2} , the conversion profiles of different cycles overlap and are parallel to each other during the fast stage and the slow stage, respectively. Fig. 6(b) also shows that the apparent rates during the fast stage and the slow stage are both higher with higher p_{CO_2} . However, the final conversion is lower in cycle 3 than in cycle 13, despite the former having a higher carbonating p_{CO_2} , because the cycling history also plays an important role in determining the sorbent's behaviour. As discussed above, the final uptake of CO₂ is mainly determined by the extent of the fast stage: the longer the fast stage lasts, the higher the overall conversion. It also appears that a higher p_{CO_2} in the preceding cycle will result in an extended fast stage, regardless of the p_{CO_2} in the subsequent cycles. When the carbonation p_{CO_2} is reduced again to 0.15 bar, the fast stage starts to shorten, resulting in a gradual fall in cyclic CO₂ uptake.

3.5. Effect of carbonation time

To investigate the effect of the carbonation time on the uptake, the recovered HAM83 (after 60 cycles in a fluidised bed) was cycled further in a TGA with various carbonation and calcination times. In the first experiment, the material was carbonated and calcined for 8 min each for 10 cycles, as in the fluidised bed experiment. Then, the carbonation and calcination times were increased to 80 and 20 min, respectively, for the subsequent 10 cycles. In the second experiment, the 10 long cycles described

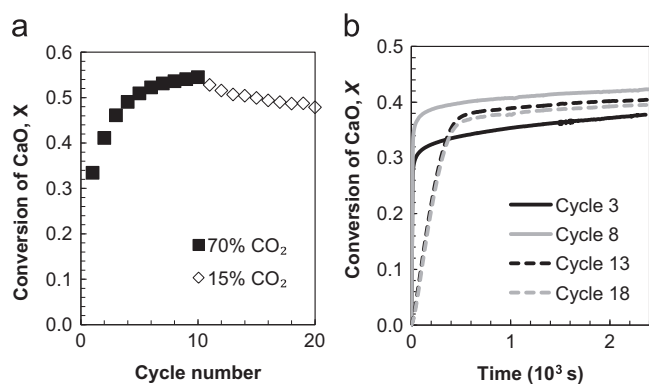


Fig. 6. Results of cycling a batch of HAM 83 in a TGA, after 60 cycles in a fluidised bed. During the first ten cycles in the TGA, the inlet gas during carbonation was 70 mol% CO_2 in N_2 . In the subsequent 10 cycles, the gas inlet during carbonation was 15 mol% CO_2 in N_2 . Calcination took place in pure N_2 . The times for carbonation and calcination are 40 min and 20 min, respectively, for all the 20 cycles. The cycling experiment took place isothermally at 750 °C. (a) shows cyclic conversion of CaO against cycle number; (b) shows conversion versus time for cycles 3, 8, 13 and 18 during carbonation.

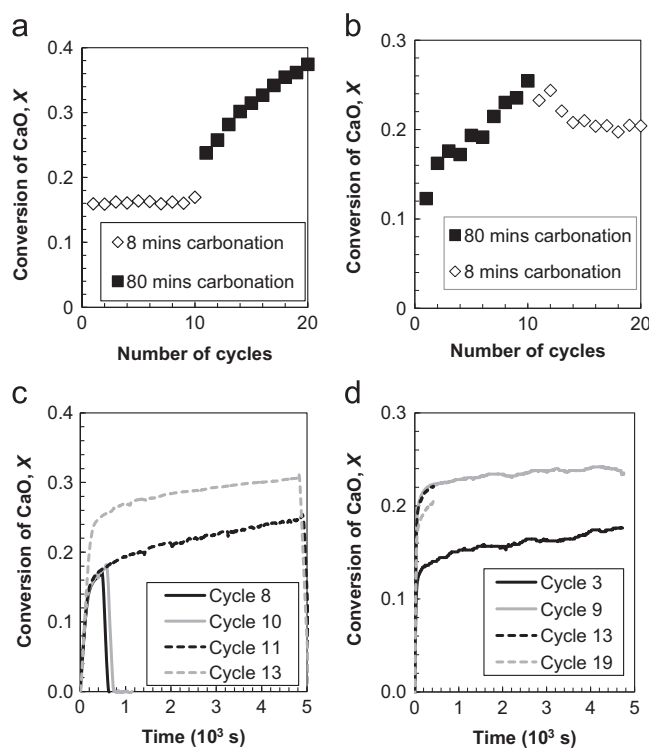


Fig. 7. Conversion of CaO versus number of cycles for a batch of HAM 83, recovered after 60 cycles in a fluidised bed, over 20 cycles in a TGA. Carbonating and calcining gases were 15 mol% CO_2 in N_2 and N_2 , respectively. All cycles were undertaken isothermally in 750 °C. The sorbent was (a) carbonated and calcined for 8 min each 10 times followed by 10 cycles with 80 min carbonation and 20 min calcination or (b) vice versa. (c) and (d) shows conversion versus time during the carbonation at selected cycles for experiments (a) and (b).

above were performed first, followed by the 10 short cycles. In both experiments, the carbonating and calcining gases were 15 mol% CO_2 in N_2 and pure N_2 , respectively. The results of the experiments are shown in Fig. 7. From Fig. 7(a), during the first ten cycles, the uptake changed little, probably because the conditions were identical to those in the first 60 cycles in the bed. When the carbonation time was increased to 80 min, the cyclic conversion of CaO increased quickly over cycles, from 0.24 in the 11th cycle to 0.37 in the 20th. When the sorbent was exposed to long and then

short carbonation times, there was a quick rise in uptake followed by a slow fall, as in Fig. 7(b).

The conversion profiles for selected cycles are shown in Fig. 7(c) and (d). It can be seen that the fast stage lasts longer when the sorbent has been carbonated for longer in the previous cycles, suggesting that deep carbonation could promote the sorbent's performance, e.g. the increase in uptake from cycle 11 to cycle 13 shown in Fig. 7(c). When the carbonation time is reduced, the fast stage in the subsequent cycles will also shorten, e.g. the decrease in uptake from cycle 13 to cycle 19 in Fig. 7(d). Combining this result with those shown in Section 3.4, it can be concluded that the change in cyclic CO_2 uptake with p_{CO_2} or carbonation time is largely a result of the cycling history of the sorbent: the deeper the carbonation, the longer the fast stage will last in the subsequent cycles. Furthermore, if the degree of carbonation is reduced, this memory effect will result in a lagged decrease in cyclic uptake by gradually shortening the fast stage over cycles. This observation differs from that of Grasa et al. (2009), who found that the performance of a limestone was more stable when carbonated less in each cycle, i.e. deeper carbonation led to severer sintering and faster deactivation. However, this argument may not be applicable to the HAM sorbents, in which sintering is considerably impeded by the inert supports, as discussed in Section 4.2 below.

3.6. Material characterisation

To relate the behaviour of the sorbents to their pore structures, the sorbents were analysed by nitrogen adsorption–desorption isotherms and scanning electron microscopy (SEM). The results of the isotherm analysis are shown in Fig. 8 and Table 2. Table 2 shows that the BET surface areas, S_{BET} , for all the samples increased over cycling. In particular, S_{BET} for HAM83, 66 and 50 almost tripled after 100 cycles in a fluidised bed, albeit at low values. For HAM100, there was only a slight increase during the

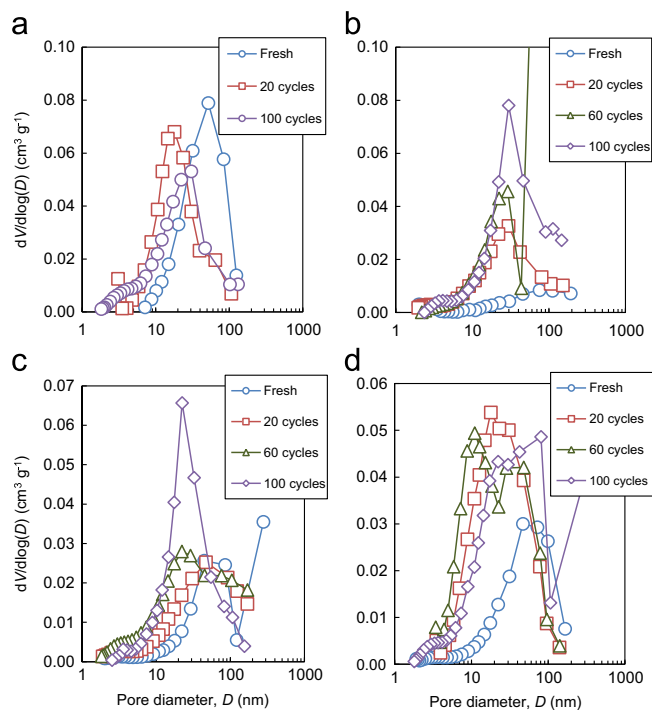


Fig. 8. Pore size distribution calculated from nitrogen adsorption–desorption isotherms, for calcined samples of (a) HAM100, (b) HAM83, (c) HAM66 and (d) HAM50. The cycles, squares, triangles and diamonds represent calcined sorbents after 0, 20, 60 and 100 cycles, respectively, in a fluidised bed.

Table 2

BET surface areas (in $\text{m}^2 \text{g}^{-1}$ sample) and BJH pore volumes ($\text{cm}^3 \text{g}^{-1}$ sample) of calcined HAM 100, 83, 66 and 50 ($1.7 < d_p < 2.4$ mm), at various stages during cycling in a fluidised bed.

Number of cycles	BET Surface Area, S_{BET} ($\text{m}^2 \text{g}^{-1}$ sample)				BJH Volume, V_{BJH} ($\text{cm}^3 \text{g}^{-1}$ sample)			
	HAM100	HAM83	HAM66	HAM50	HAM100	HAM83	HAM66	HAM50
0	8.5	2.6	2.7	3.3	0.072	0.009	0.020	0.025
20	9.6	6.3	4.5	7.7	0.048	0.028	0.026	0.049
60	–	6.7	6.7	8.8	–	0.053	0.034	0.052
100	9.0	7.8	6.3	9.0	0.043	0.055	0.039	0.055

first 20 cycles, followed by a decrease from cycle 20 to cycle 100. However, the magnitude of the increase for HAM100 is comparable to typical experimental uncertainties in BET measurements, viz. $\sim 1 \text{ m}^2 \text{g}^{-1}$, i.e. S_{BET} of HAM100 had not changed significantly over the cycles. The variation of BJH pore volume, V_{BJH} , somewhat reflects the change in S_{BET} for HAM83, 66 and 50, all of which show increases in V_{BJH} over cycles. For HAM100, V_{BJH} decreased over cycling despite the approximately constant S_{BET} . Overall, no sample can be considered particularly porous, which typically means $S_{\text{BET}} > 20 \text{ m}^2 \text{g}^{-1}$.

From Fig. 8, it can be seen that the pore volumes in the freshly-calcined sorbents are low. With cycling, the pore size distributions evolved substantially. For HAM100, the peak of the distribution shifted from a diameter of ~ 50 nm to ~ 20 nm after 20 cycles and stayed around 20 nm until the 100th cycle. There also seems to be a decrease in the total pore volume over cycles, as suggested by the decrease in the area under the curve; this is in agreement with the results shown in Table 2. For HAM83, the porosity keeps increasing throughout the 100 cycles. The pore size distributions for HAM66 and 50 exhibit the most increase between cycle 60 and 100, and cycle 0–20, respectively.

Overall, in all samples, cycling promoted porosity, especially for pores with diameter ~ 20 nm. Because the isothermal N_2 adsorption–desorption analysis only measures pores smaller than 200 nm in diameter, the macroporosity of the samples was examined qualitatively using SEM. Fig. 9(a) – (d) and (e) – (h) shows the evolution of surface morphologies of the calcined HAM100 and 83, respectively, with cycling in a fluidised bed. High resolution images of the SEM images are shown in Supplementary material. In both sorbents, the freshly calcined samples consist of agglomerates of small grains of diameter $\sim 1 \mu\text{m}$. On cycling, the grains grew whilst the voids between the grains, viz. the macropores, shrank. This is especially the case for HAM100, where severe sintering is seen after only 20 cycles. In fact, from cycle 20 to cycle 100, little further morphological change is seen. For HAM83, shown in Fig. 9(h), the macroporosity also appears heavily reduced after 100 cycles. In addition, cracks can be seen on the surface of both cycled sorbents. In HAM83, the cracks are large and have split entire grains, as shown in Fig. 9(f) and (g), whereas for HAM100, the cracks are in the form of small fissures on the sintered surfaces. The surfaces of the particles of HAM83, in their carbonated state at various stages during cycling, are shown in Fig. 9(i)–(l): no cracks can be seen, indicating that the cracks were created during calcination and cured in the subsequent carbonation. Furthermore, some macroporosity remains in the carbonated HAM83 (Fig. 9(l)), suggesting that the lack of macroporosity seen in Fig. 9(h) may not be representative of particles of HAM83, the core of which may still be accessible by CO_2 via molecular gaseous diffusion after the 100 cycles.

4. Discussion

4.1. Behaviour of sorbents during carbonation

Carbonation is significantly slower than calcination. Therefore, the rate of carbonation is the factor limiting the cyclic uptake. The results of the TGA experiments (Fig. 5) show that, for all synthetic sorbents, the carbonation undergoes two stages: a fast stage and a slow stage. During the fast stage, the conversion increases approximately linearly with time, a result of the fact that the apparent rates are controlled by external mass transfer (from the bulk gas phase to the surface of the particles) in the TGA, as demonstrated by Liu et al. (2012a). This may not be the case in a fluidised bed, in which the rate of external mass transfer is faster. However, the fluidised bed experiments are not sensitive enough to register the transition between the fast and the slow stages. Therefore, to investigate this transition, which appears to be the factor determining CO_2 uptake, the discussion in this section will focus on the results in Sections 3.3–3.6.

Another interesting feature in Fig. 5 are the linear and parallel conversion profiles during the slow stage for HAM50 and 83, suggesting that these rates are independent of the conversion achieved during the fast stage. This means the kinetics of the two stages are determined by different properties of the sorbent. Nevertheless, the extent of the slow stage, i.e. the degree of carbonation, affects the property determining the extent of the fast stage in the subsequent cycle.

Here, a connection between the observations in Figs. 8 and 9 can be made, viz. the small cracks on the surface of the cycled particles might be responsible for the growth in mesoporosity. In the literature, the fast-stage of the carbonation reaction is usually associated with the filling of the mesopores in the calcined sorbents, whilst the slow stage corresponds to product layer thickening on the large grains via solid state diffusion. Therefore, the properties which determine the kinetics of the fast and the slow stages should be the mesoporosity, generated by surface cracking, and the macroporosity, respectively. In fact, surface cracking during calcination is a well-known phenomenon in Ca-based sorbents (Fennell et al., 2007; Valverde et al., 2014) and its ability to create pores has been utilised to enhance the performance of both natural and synthetic sorbents (Blamey et al., 2010; Stendardo et al., 2013).

Based on the experimental evidence, an explanation of the behaviour of the synthetic sorbents is proposed and depicted in Fig. 10. Initially, the freshly-calcined sample (state (a) in Fig. 10) contains “smooth” grains containing little porosity. On exposure to CO_2 , the grains are quickly covered by a thin layer of CaCO_3 after the initial nucleation. The calcite layer keeps thickening, until it reaches a critical thickness, δ_c , at which point the rate is significantly slowed by the resistance to diffusion of CO_2 through the product layer to the unreacted core of CaO , i.e., state (c) in Fig. 10. Here, it is postulated that the growing layer is roughly continuous, composed of closely-packed grains, as suggested by the work of Li

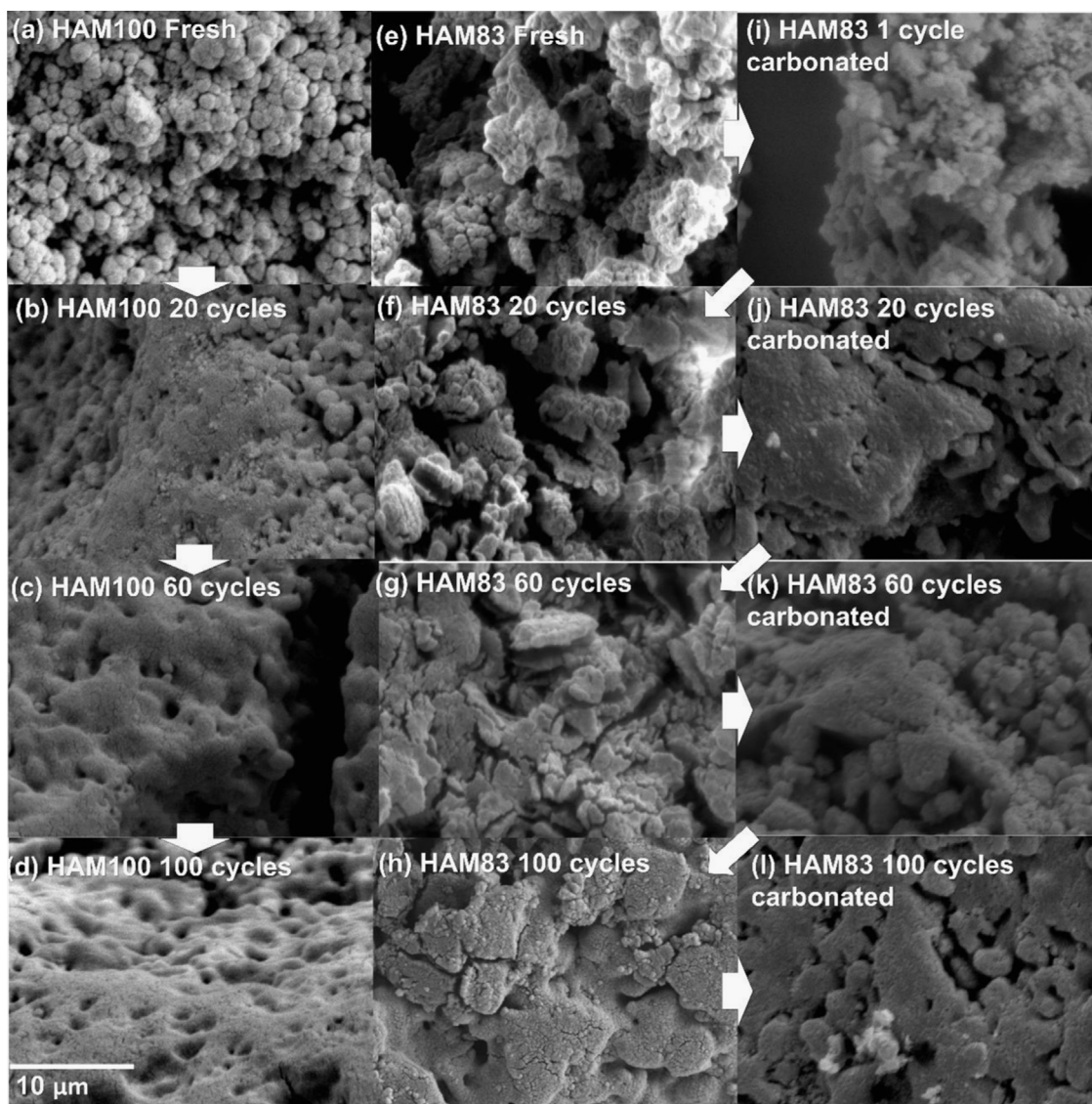


Fig. 9. SEM images of the surface of particles of (a)–(d) calcined HAM100, (e)–(h) calcined HAM83 and (i)–(l) carbonated HAM83 after different number of cycles in a fluidised bed with 8 min carbonation in 15 mol% CO_2 in N_2 and 8 min calcination in pure N_2 in each cycle at 750 °C. The arrows indicate the sequence in time when the samples were recovered. All micrographs have the same scale, shown at the bottom left.

et al. (2012). Beyond this point, the reaction transforms from the fast stage to the slow stage, in which the rate is effectively controlled by product layer diffusion, until the end of the carbonation. During calcination, the grains of CaCO_3 decompose and contract rapidly, generating large tensile stresses across the calcite layer, *i.e.* states (d)–(f). Consequently, cracks are created, together with additional mesoporosity and surface area, which means the sorbent can accommodate more CaCO_3 during the fast stage in the next cycle. With deeper carbonation, more calcite is available for cracking and generation of additional surface area, hence a higher uptake during the fast stage is expected in the subsequent cycle. As long as the structure of the macro-pores remains stable, the slow stage is unaffected by the cracks (the mesopores), which would have been filled after the fast stage. That is to say states (c) and (g) in Fig. 10 are effectively identical with respect to the reacting CO_2 during the slow stage. Therefore, the rates during the slow stage are independent of the conversion achieved during the fast stage.

HAM66 and 50 exhibit behaviour similar to that of HAM83, except for the lower cyclic uptakes. However, after normalising the

sorbents' uptakes with respect to those in the first cycle, as shown in Fig. 11, HAM50 was found, on this basis, to be the best over the 100 cycles, followed by HAM66 and HAM83. The trends shown in Fig. 11(a) and (b) suggest that, with higher contents of mayenite and MgO, the uptake increases by a larger fraction over cycling, *i.e.* the addition of the support materials enhances the surface cracking. Furthermore, the initial conversion of CaO appears to decrease with decreasing content of CaO, suggesting that the rate of carbonation is retarded by the support material. Nevertheless, the mayenite and MgO do not actually reduce the total amount of CaO available for carbonation, as shown by the *in situ* sXRD results.

It might be the case that rapid decomposition is an essential condition to induce surface cracking. Therefore, the likelihood of surface cracking under what is likely to be a realistic calcination condition, *e.g.* 900 °C in 1 bar CO_2 , is discussed here. Khinast et al. (1996) measured the rate of decomposition of limestone and described the results using a pore model (Bhatia and Perlmutter, 1980, 1981), which suggests the feasibility of surface cracking in 0.065 bar CO_2 at 780 °C. Additionally, according to a simple extrapolation using the existing rate expressions and kinetic

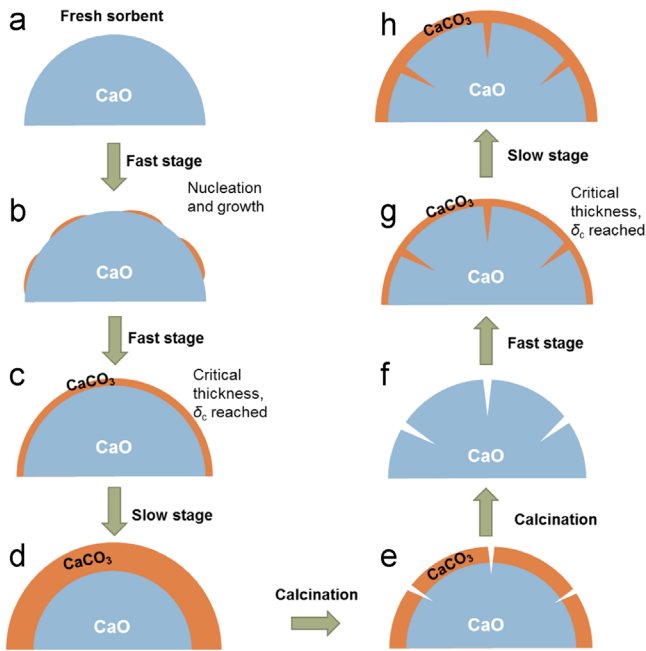


Fig. 10. A schematic diagram demonstrating the change in morphology over 1.5 cycles of calcium looping of a fresh CaO sorbent. The nucleation and growth during carbonation in the second cycle is not shown for brevity.

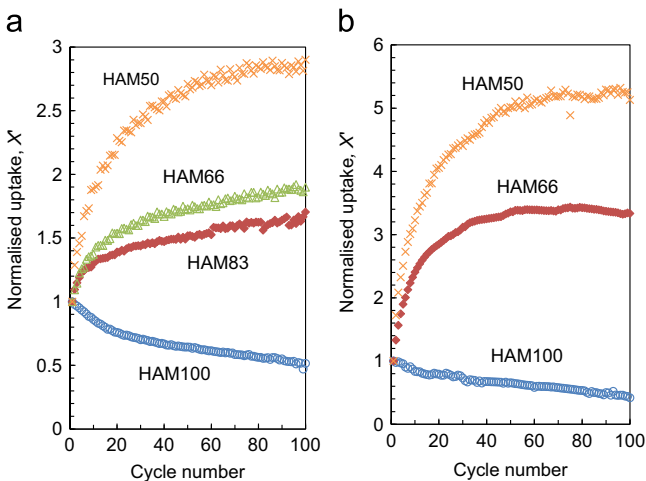


Fig. 11. Normalised uptake of CO₂ by different synthetic sorbents during 100 cycles in (a) fluidised bed and (b) TGA at 750 °C. In the fluidised bed, the sorbents are carbonated in 15% CO₂ in N₂ for 8 min and calcined in N₂ for 8 min in each cycle. In the TGA, the sorbents are carbonated in 15% CO₂ in N₂ for 40 min and calcined in N₂ for 20 min in each cycle.

parameters in the literature (Ioannou et al., 2009; Stanmore and Gilot, 2005), the rate of calcination in 900 °C and 1 bar CO₂ should be much faster than that observed by Khinast et al. (1996) and thus fast enough to cause surface cracking. Nevertheless, there is still the possibility of the synthetic sorbents performing worse when subjected to high p_{CO_2} and temperature during calcination, owing to factors such as sintering, as demonstrated by Broda et al. (2012) using a synthetic sorbent with a composition similar to HAM83. Furthermore, surface cracking may play a less important role in synthetic sorbents with high initial uptakes, e.g. those developed by Broda et al. (2014) and Broda and Müller (2014), in which a large portion of the CaO is already accessible by CO₂ in the first cycle.

4.2. Role of sintering

Sintering also plays an important role in altering the reactivity of the synthetic sorbents over cycles. Because surface cracking is a recurring process, i.e. mesoporosity is regenerated during calcination in every cycle, sintering only irreversibly reduces the macroporosity. As discussed above, the severity of sintering is reflected by carbonation during the slow stage, the rate of which is determined by the macroporosity.

Amongst the synthetic sorbents, sintering affected HAM100 the most, as suggested by Fig. 5(a) where the cyclic uptake decreased steadily with increasing numbers of cycles. The reaction model for the slow stage developed by Liu et al. (2012b) suggests that the slowing rate corresponds to grain growth, agreeing with the surface morphologies observed in Fig. 9. The overall reduction in cyclic uptake also means the additional uptake due to the small fissures seen in Fig. 9(b–d) is negligible compared to the reduction in reactivity due to sintering. In fact, severe sintering is expected for HAM100, especially when it is carbonated, because the Tamman temperature (the temperature above which sintering is expected to be severe) of CaCO₃ (533 °C) is much below the operation temperature of 750 °C. In contrast, the material is less likely to sinter when calcined, because the Tamman temperature of CaO is 1170 °C.

For HAM83, the presence of mayenite and MgO is expected to resist sintering, despite the low Tamman temperature of mayenite of 546 °C, because the CaCO₃ and the mayenite will mutually exert Zener pinning force on each other (Smith, 1948). Indeed, after the first 20 cycles, sintering seems to have stabilised, as suggested by the consistent rates during the slow stage seen in Fig. 5(b) and the SEM images in Fig. 9. Meanwhile, surface cracking during calcination brought additional uptake in each cycle. Nevertheless, there has been some sintering during the first few cycles, as manifested by the decrease in rates during the slow stage for cycles 1–5 (Fig. 5(b)) and the disappearance of the small grains in the fresh sorbents (Fig. 9(a)). Overall, the extent of sintering in HAM83 was small compared to HAM100 and has stabilised after the first few cycles.

The development of strain prior to cracking is also influenced by the curvature of the carbonated surface, i.e. more curvature corresponds to larger strains and therefore greater tendencies to crack. Therefore, the highly-sintered surface of the cycled HAM100 is expected to crack less than that of the cycled HAM83; this is indeed the case shown in Fig. 9. Therefore, surface cracking is more effective in promoting the sorbents' performance when the macroporosity is preserved, e.g. by the addition of mayenite and MgO.

4.3. Implication of the reaction model

In this section, a qualitative correlation between S_{BET} , V_{BJH} and uptake during the fast stage is proposed. First, it is assumed that the uptake measured in the fluidised bed experiment corresponds to the extent of the fast stage, which can be described by a process of either (i) filling up the BJH pores (pore diameter < 200 nm) or (ii) the development of a thin layer of CaCO₃. In the former case, the CO₂ uptake, X'' , expressed in unit mass of CO₂ per unit mass of sorbent, is related to V_{BJH} by:

$$X'' = \frac{V_{\text{BJH}} \cdot \rho_{\text{CaO}} M_{\text{CO}_2}}{1/Z - 1 M_{\text{CaO}}} \quad (1)$$

where $\rho_{\text{CaO}} = 3.32 \text{ g cm}^{-3}$ is the mass density of CaO, M_i is the molecular mass of species i and $Z = 0.46$ is the ratio of molar volume of CaO to CaCO₃ at 750 °C, calculated by interpolating the refined cell parameters at 600 and 900 °C using the XRD results. Accordingly, the uptakes calculated using the measured V_{BJH} are compared to the experimentally-determined uptakes in Fig. 12, the

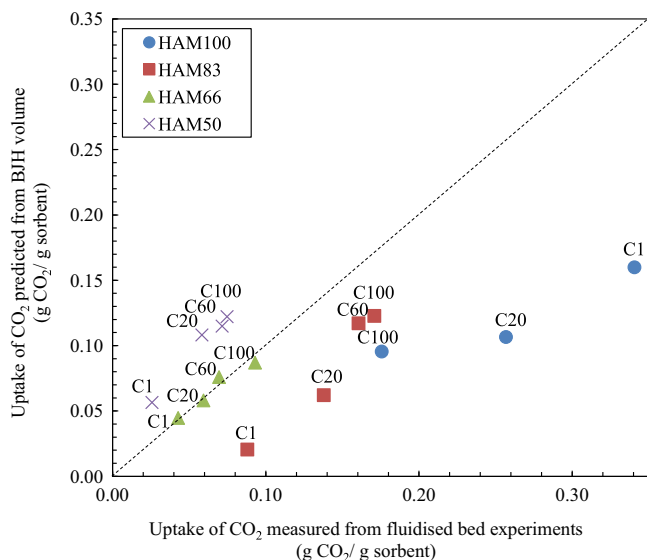


Fig. 12. Uptake of CO₂ predicted by filling of BJH pores versus experimental measurements, for the four synthetic sorbents at various stages of the cycling experiment in the fluidised bed. The numbers following the letter C indicate the numbers of cycles at which the measurements were made. The diagonal line corresponds to the ideal case in which the prediction is perfect.

Table 3

Surface area (in m² g⁻¹ sample) and volume fraction of CaO of calcined HAM 100, 83, 66 and 50 (1.7 < d_p < 2.4 mm), at various stages during cycling in a fluidised bed.

Number of cycles	HAM100	HAM83	HAM66	HAM50
0	8.5	2.3	1.9	1.8
20	9.6	5.5	3.1	4.1
60	–	5.9	4.7	4.7
100	9.0	6.9	4.4	2.5
ν_{CaO}	1.0	0.88	0.70	0.53

plot showing that, in general, X' is positively correlated with V_{BJH} . However, the pore-filling model underestimates the uptake by HAM100 and HAM83, suggesting that the carbonation continued after the mesopores were completely filled, *i.e.* the reaction continued beyond the fast stage. This is expected as the transition to the slow stage may have happened within the 8 min of carbonation, as shown in Fig. 5. For HAM66, the uptake is predicted exactly by Eq. (1), whereas for HAM50 the uptake is overestimated by the model, suggesting its BJH pores have not been filled completely by the end of the carbonation. One possible reason for the measured uptake by HAM50 being lower than that calculated using Eq. (1) is pore-plugging, which makes some fraction of the mesopores inaccessible by CO₂ during the fast stage. In addition, the presence of pore plugging might affect the kinetics during the slow stage. Undoubtedly, an ideal CaO-based sorbent should have mesoporosity that is large enough to accommodate the complete conversion of CaO and stable over a large number of cycles.

Alternatively the fast stage could be regarded as the development of a layer of product covering the surface of CaO. If the product layer is thin, the uptake should be approximately proportional to the surface area of CaO in the calcined sorbent, S_{CaO} . Assuming CaO is homogeneously dispersed in the synthetic sorbents, $S_{\text{CaO}} \approx \nu_{\text{CaO}} \times S_{\text{BET}}$, where ν_{CaO} is the volume fraction of CaO. Here, the values of ν_{CaO} and S_{CaO} for the sorbents at various stages of cycling are shown in Table 3. Accordingly, the measured uptake is plotted against S_{CaO} in Fig. 13, which shows that, for the three synthetic sorbents with MgO and mayenite, the uptake can be linearly correlated S_{CaO} . Therefore, for a given material in a given

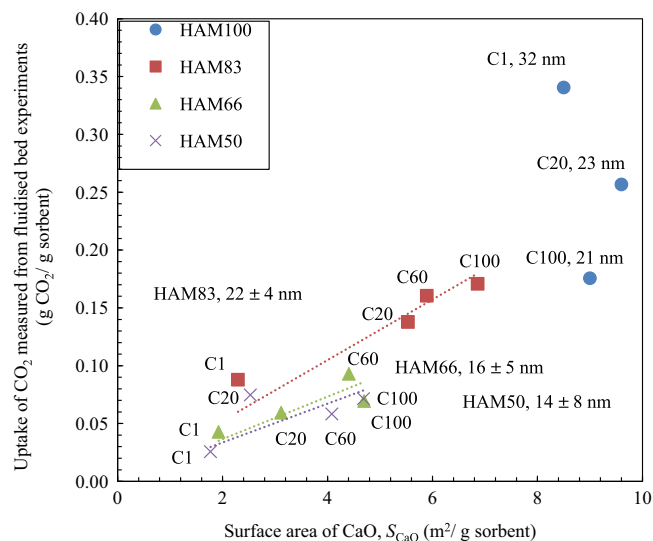


Fig. 13. Uptake of CO₂ measured in a fluidised bed versus surface area of CaO, for the four synthetic sorbents at various stages of calcium looping cycles in a fluidised bed. The numbers following the letter C indicate the numbers of cycles at which the measurements were made. The values of the product layer thickness, δ are calculated based on the gradients of the linear fits through the origin; the errors correspond to 95% confidence bands of δ .

period of time, the thickness of the product layer, δ can be calculated from the gradient of a line through the origin, fitted to the points in Fig. 13, by

$$\delta = \frac{V_{\text{CaCO}_3} X''}{M_{\text{CO}_2} S_{\text{CaO}}}, \quad (2)$$

where V_{CaCO_3} is the mass density of CaCO₃. The constant value of δ suggests that the growth of the product layer is significantly slowed after reaching a critical value, *i.e.* $\delta = \delta_c$; this observation is in agreement with the model in Fig. 10. Given the error in the estimated values of δ_c , HAM83, HAM66 and HAM50 appear to have similar critical product layer thicknesses. For HAM100, the product layer developed in the first cycle is thicker than those in the subsequent cycles, suggesting the reactivity of the fresh HAM100 may be chemically different to that of the cycled HAM100 and the supported sorbents. All the values of δ_c estimated for the synthetic sorbents are lower than the ~50 nm determined for natural sorbents by Alvarez and Abanades (2005), who were also able to correlate the BET surface area with the uptake for four limestones under a variety of operating conditions.

The reaction model established in the present study may also be applicable to the synthetic sorbent HA-85-850, developed and investigated by Pacciani et al. (2008b), Dennis and Pacciani (2009) and Liu et al. (2012b). Furthermore, for natural sorbents exhibiting the two-stage behaviour during carbonation, the effect of deep-carbonation on the performance in the subsequent cycles has also been reported. For example, Lysikov et al. (2007) and Sun et al. (2008) found that prolonged carbonation would improve the cyclic uptake by CaO *c.f.* the rapidly deteriorating performance reported by Grasa and Abanades (2006). Arias et al. (2012) found that the reactivity of a limestone was considerably improved when a step to carbonate the limestone in $p_{\text{CO}_2} = 1$ atm at 800 °C was introduced after the conventional carbonation in each cycle. The apparent similarity between the responses by the natural and the synthetic sorbents to deep carbonation means that the reaction model also offers an explanation to the observations above with the natural sorbents.

5. Conclusion

In this work, sorbents of CO₂, consisting of CaO supported on Ca₁₂Al₁₄O₃₃ (mayenite) and MgO, were synthesised using a method starting by hydrolysing CaO. The behaviour of the synthesised sorbents, viz. HAM100, 83, 66 and 50 over calcium looping cycles (for post-combustion capture of CO₂) were investigated experimentally. Under the operating conditions used, the final uptake in each cycle is determined by the rate of carbonation. During carbonation, the reaction proceeds firstly via a fast stage, the extent of which is related to the availability of surface area and mesoporosity. After the growth of a layer of product CaCO₃ of a critical thickness, the reaction switches to a slow stage, the rate of which is determined by the diffusion of CO₂ through the product layer.

It was found that for pure CaO, i.e. HAM100, the cyclic uptake degrades over cycles, as it loses porosity because of sintering. For synthetic sorbents with some sintering resistance, i.e. HAM83, 66 and 50, the uptake increases over cycling, because of the development of mesoporosity and additional surface area by a surface cracking mechanism. It is proposed that the surfaces of the sorbents crack as a result of high mechanical stress caused by the drastic change in molar volume during the calcination. In conclusion, the self-regenerating mesoporosity due to surface cracking is the key to the outstanding performance of the supported synthetic sorbents.

Acknowledgements

The authors would like to thank the Australian Synchrotron for the award of beamtime, and Justin Kimpton and Qinfen Gu for their help with the design and operation of the in situ gas flow capillary XRD cell. Mr Zlatko Zaracevic is acknowledged for the BET measurements. W.L acknowledges funding from the National Research Foundation (NRF), Prime Minister's Office, Singapore under its Campus for Research Excellence and Technological Enterprise (CREATE) programme. B.G acknowledges the EU Research Fund for Coal and Steel (project number RFCR-CT-2012-00008). M.T.D acknowledges funding from the Cambridge Commonwealth Trusts and Trinity College, Cambridge and the EU ERC for an advanced fellowship for CPG. D.S.S acknowledges financial support by Engineering and Physical Sciences Research Council (EPSRC). C.D.L acknowledges funding by the Australian Research Council (Discovery Projects).

Appendix A. Supplementary material

Supplementary data associated with this article can be found in the online version at <http://dx.doi.org/10.1016/j.ces.2015.09.016>.

References

- Abanades, J.C., Alvarez, D., 2003. Conversion limits in the reaction of CO₂ with lime. *Energy Fuels* 17, 308–315. <http://dx.doi.org/10.1021/ef020152a>.
- Alvarez, D., Abanades, J.C., 2005. Determination of the critical product layer thickness in the reaction of CaO with CO₂. *Ind. Eng. Chem. Res.* 44, 5608–5615. <http://dx.doi.org/10.1021/ie050305s>.
- Anthony, E.J., 2008. Solid looping cycles: a new technology for coal conversion. *Ind. Eng. Chem. Res.* 47, 1747–1754. <http://dx.doi.org/10.1021/ie071310u>.
- Arias, B., Grasa, G.S., Alonso, M., Abanades, J.C., 2012. Post-combustion calcium looping process with a highly stable sorbent activity by recarbonation. *Energy Environ. Sci.* 5, 7353–7359. <http://dx.doi.org/10.1039/C2EE03008J>.
- Barker, R., 1973. The reversibility of the reaction CaCO₃ ⇌ CaO + CO₂. *J. Appl. Chem. Biotechnol.* 23, 733–742. <http://dx.doi.org/10.1002/jctb.5020231005>.
- Barrett, E.P., Joyner, L.G., Halenda, P.P., 1951. The determination of pore volume and area distributions in porous substances. I. Computations from nitrogen isotherms. *J. Am. Chem. Soc.* 73, 373–380. <http://dx.doi.org/10.1021/ja01145a126>.
- Bhatia, S.K., Perlmutter, D.D., 1983. Effect of the product layer on the kinetics of the CO₂-lime reaction. *AIChE J.* 29, 79–86. <http://dx.doi.org/10.1002/aic.690290111>.
- Bhatia, S.K., Perlmutter, D.D., 1981. A random pore model for fluid-solid reactions: II. Diffusion and transport effects. *AIChE J.* 27, 247–254. <http://dx.doi.org/10.1002/aic.690270211>.
- Bhatia, S.K., Perlmutter, D.D., 1980. A random pore model for fluid-solid reactions: I. Isothermal, kinetic control. *AIChE J.* 26, 379–386. <http://dx.doi.org/10.1002/aic.690260308>.
- Blamey, J., Paterson, N.P.M., Dugwell, D.R., Fennell, P.S., 2010. Mechanism of particle breakage during reactivation of CaO-based sorbents for CO₂ capture. *Energy Fuels* 24, 4605–4616. <http://dx.doi.org/10.1021/ef100476d>.
- Broda, M., Kierzkowska, A.M., Müller, C.R., 2014. Development of highly effective CaO-based, MgO-stabilized CO₂ Sorbents via a scalable “One-Pot” recrystallization technique. *Adv. Funct. Mater.* 24, 5753–5761. <http://dx.doi.org/10.1002/adfm.201400862>.
- Broda, M., Kierzkowska, A.M., Müller, C.R., 2012. Influence of the calcination and carbonation conditions on the CO₂ uptake of synthetic Ca-based CO₂ sorbents. *Environ. Sci. Technol.* 46, 10849–10856. <http://dx.doi.org/10.1021/es302757e>.
- Broda, M., Müller, C.R., 2014. Sol-gel-derived, CaO-based, ZrO₂-stabilized CO₂ sorbents. *Fuel, fluidized bed combustion and gasification – CO₂ and SO₂ capture: Special issue in honor of Professor E.J. (Ben) Anthony 127*, pp. 94–100. [10.1016/j.fuel.2013.08.004](http://dx.doi.org/10.1016/j.fuel.2013.08.004).
- Broda, M., Müller, C.R., 2012. Synthesis of highly efficient, Ca-based, Al₂O₃-stabilized, carbon gel-templated CO₂ sorbents. *Adv. Mater.* 24, 3059–3064. <http://dx.doi.org/10.1002/adma.201104787>.
- Brunauer, S., Emmett, P.H., Teller, E., 1938. Adsorption of gases in multimolecular layers. *J. Am. Chem. Soc.* 60, 309–319.
- Davies, R., Dinsdale, A., Gisby, J., Robinson, J., Martin, S., 2002. MTDATA-thermodynamic and phase equilibrium software from the national physical laboratory. *Calphad* 26, 229–271. [http://dx.doi.org/10.1016/S0364-5916\(02\)00036-6](http://dx.doi.org/10.1016/S0364-5916(02)00036-6).
- Dennis, J.S., Pacciani, R., 2009. The rate and extent of uptake of CO₂ by a synthetic, CaO-containing sorbent. *Chem. Eng. Sci.* 64, 2147–2157. <http://dx.doi.org/10.1016/j.ces.2009.01.051>.
- Doman, R.C., Barr, J.B., McNally, R.N., Alper, A.M., 1963. Phase equilibria in the system CaO–MgO. *J. Am. Ceram. Soc.* 46, 313–316. <http://dx.doi.org/10.1111/j.1151-2916.1963.tb11737.x>.
- Fennell, P.S., Pacciani, R., Dennis, J.S., Davidson, J.F., Hayhurst, A.N., 2007. The effects of repeated cycles of calcination and carbonation on a variety of different limestones, as measured in a hot fluidized bed of sand. *Energy Fuels* 21, 2072–2081. <http://dx.doi.org/10.1021/ef060506o>.
- Grasa, G., Abanades, J.C., Anthony, E.J., 2009. Effect of partial carbonation on the cyclic CaO carbonation reaction. *Ind. Eng. Chem. Res.* 48, 9090–9096. <http://dx.doi.org/10.1021/ie900443y>.
- Grasa, G.S., Abanades, J.C., 2006. CO₂ capture capacity of CaO in long series of carbonation/calcination cycles. *Ind. Eng. Chem. Res.* 45, 8846–8851. <http://dx.doi.org/10.1021/ie0606946>.
- Gupta, H., Fan, L.-S., 2002. Carbonation–calcination cycle using high reactivity calcium oxide for carbon dioxide separation from flue gas. *Ind. Eng. Chem. Res.* 41, 4035–4042. <http://dx.doi.org/10.1021/ie010867l>.
- Ioannou, Z., Zoumpoulakis, L., Halikias, I., Teloniati, T., 2009. Overall kinetic study of non-isothermal decomposition of calcium carbonate. *Miner. Process. Extr. Metall. Trans. Inst. Min. Metall. Sect. C* 118, 98–104. <http://dx.doi.org/10.1179/174328509X393240>.
- Khinast, J., Krammer, G.F., Brunner, C., Staudinger, G., 1996. Decomposition of limestone: the influence of CO₂ and particle size on the reaction rate. *Chem. Eng. Sci.* 51, 623–634. [http://dx.doi.org/10.1016/0009-2509\(95\)00302-9](http://dx.doi.org/10.1016/0009-2509(95)00302-9).
- Larson, A.C., Von Dreele, R.B., 2000. General Structure Analysis System (GSAS), Los Alamos National Laboratory Report LAUR pp. 86–748.
- Liu, W., Dennis, J.S., Scott, S.A., 2012a. The effect of addition of ZrO₂ to Fe₂O₃ for hydrogen production by chemical looping. *Ind. Eng. Chem. Res.* 51, 16597–16609. <http://dx.doi.org/10.1021/ie302626x>.
- Liu, W., Dennis, J.S., Sultan, D.S., Redfern, S.A.T., Scott, S.A., 2012b. An investigation of the kinetics of CO₂ uptake by a synthetic calcium based sorbent. *Chem. Eng. Sci.* 69, 644–658. <http://dx.doi.org/10.1016/j.ces.2011.11.036>.
- Li, Z., Cai, N., Huang, Y., Han, H., 2005. Synthesis, experimental studies, and analysis of a new calcium-based carbon dioxide absorbent 1999–2004.
- Li, Z., Fang, F., Tang, X., Cai, N., 2012. Effect of temperature on the carbonation reaction of CaO with CO₂. *Energy Fuels* 26, 2473–2482. <http://dx.doi.org/10.1021/ef201543n>.
- Lysikov, A.I., Salanov, A.N., Okunev, A.G., 2007. Change of CO₂ carrying capacity of CaO in isothermal recarbonation–decomposition cycles. *Ind. Eng. Chem. Res.* 46, 4633–4638. <http://dx.doi.org/10.1021/ie0702328>.
- Pacciani, R., Müller, C.R., Davidson, J.F., Dennis, J.S., Hayhurst, A.N., 2008a. Synthetic Ca-based solid sorbents suitable for capturing CO₂ in a fluidized bed. *Can. J. Chem. Eng.* 86, 356–366. <http://dx.doi.org/10.1002/cjce.20060>.
- Pacciani, R., Müller, C.R., Davidson, J.F., Dennis, J.S., Hayhurst, A.N., 2008b. Synthetic Ca-based solid sorbents suitable for capturing CO₂ in a fluidized bed. *Can. J. Chem. Eng.* 86, 356–366. <http://dx.doi.org/10.1002/cjce.20060>.
- Silaban, A., Narcida, M., Harrison, D.P., 1996. Characteristics of the reversible reaction between CO₂ (g) and calcined dolomite. *Chem. Eng. Commun.* 146, 149–162.

- Smith, C.S., 1948. Grains, phases, and interfaces—an interpretation of microstructure. *Trans. AIME*, 15–51.
- Stanmore, B.R., Gilot, P., 2005. Review—calcination and carbonation of limestone during thermal cycling for CO₂ sequestration. *Fuel Process. Technol.* 86, 1707–1743. <http://dx.doi.org/10.1016/j.fuproc.2005.01.023>.
- Stendardo, S., Andersen, L.K., Hecce, C., 2013. Self-activation and effect of regeneration conditions in CO₂–carbonate looping with CaO–Ca₁₂Al₁₄O₃₃ sorbent. *Chem. Eng. J.* 220, 383–394. <http://dx.doi.org/10.1016/j.cej.2013.01.045>.
- Sun, P., Lim, C.J., Grace, J.R., 2008. Cyclic CO₂ capture by limestone-derived sorbent during prolonged calcination/carbonation cycling. *AIChE J.* 54, 1668–1677. <http://dx.doi.org/10.1002/aic.11491>.
- Toby, B.H., 2001. *EXPGUI*, a graphical user interface for GSAS. *J. Appl. Crystallogr.* 34, 210–213. <http://dx.doi.org/10.1107/S0021889801002242>.
- Valverde, J.M., Sanchez-Jimenez, P.E., Perez-Maqueda, L.A., Quintanilla, M.A.S., Perez-Vaquero, J., 2014. Role of crystal structure on capture by limestone derived CaO subjected to carbonation/recarbonation/calcination cycles at Ca-looping conditions. *Appl. Energy* 125, 264–275. <http://dx.doi.org/10.1016/j.apenergy.2014.03.065>.
- Wen, C.Y., Yu, Y.H., 1966. A generalized method for predicting the minimum fluidization velocity. *AIChE J.* 12, 610–612. <http://dx.doi.org/10.1002/aic.690120343>.